

Neural Fidelity Calibration for Informative Sim-to-Real Adaptation

Youwei Yu, Lantao Liu

Abstract—Deep reinforcement learning can seamlessly transfer agile locomotion and navigation skills from the simulator to real world. However, bridging the sim-to-real gap with domain randomization or adversarial methods often demands expert physics knowledge to ensure policy robustness. Even so, cutting-edge simulators may fall short of capturing every real-world detail, and the reconstructed environment may introduce errors due to various perception uncertainties. To address these challenges, we propose Neural Fidelity Calibration (NFC), a novel framework that employs conditional score-based diffusion models to calibrate simulator physical coefficients and residual fidelity domains online during robot execution. Specifically, the residual fidelity reflects the simulation model shift relative to the real-world dynamics and captures the uncertainty of the perceived environment, enabling us to sample realistic environments under the inferred distribution for policy fine-tuning. Our framework is informative and adaptive in three key ways: (a) we fine-tune the pretrained policy only under anomalous scenarios, (b) we build sequential NFC online with the pretrained NFC’s proposal prior, reducing the diffusion model’s training burden, and (c) when NFC uncertainty is high and may degrade policy improvement, we leverage optimistic exploration to enable “hallucinated” policy optimization. Our framework achieves superior simulator calibration precision compared to state-of-the-art methods across diverse robots with high-dimensional parametric spaces. We study the critical contribution of residual fidelity to policy improvement in simulation and real-world experiments. Notably, our approach demonstrates robust robot navigation under challenging real-world conditions, such as a broken wheel axle on snowy surfaces.

I. INTRODUCTION

Zero-shot sim-to-real reinforcement learning (RL) has empowered agile policy to various robots across soft [74], wheeled [83], aerial [18], and quadruped [45] embodiments. In the context of policy resilience against the real-world diversities, the proximal works in domain randomization (DR) [75] and adversarial training [19] emerge as powerful strategies by artificially introducing noise or attacks into the agent’s states. Safety RL, which incorporates safety constraints into the optimization [10], remains tied to DR via exploration of diverse unsafe scenarios.

Despite these advancements, expert real-world knowledge is often required to determine domain ranges [48], reconstruct environments [15], or design adversarial scenarios [66]. In theory, one could uniformly sample every domain parameter and environment variation, but this is usually impractical. Continual online learning with offline RL bootstrapping offers a promising alternative by allowing policy adaptation from

pretrained capabilities [72]. Coupled with the sim-to-real-to-sim strategy [15], it mitigates safety risks and encourages policy improvement through extensive exploration in a reconstructed virtual world. Simulation-based inference (SBI) [57] can further refine policy fine-tuning within a narrowed DR range, balancing randomness and performance by estimating physical parameters from real-world data. However, SBI typically assumes a perfectly calibrated simulator capable of replicating real-world dynamics. Moreover, sensor data used for environmental reconstruction is prone to perception errors, such as snowy surfaces.

To address these challenges, we propose Neural Fidelity Calibration (NFC), which employs conditional score-based diffusion models to simultaneously calibrate simulator physical coefficients and residual fidelity domains online during robot execution. The residual fidelity reflects how the simulator diverges from real-world dynamics while capturing the uncertainty of the perceived environment, enabling realistic environment sampling under the inferred distribution. For informative policy adaptation, our key contributions include:

- **Neural Fidelity Calibration (NFC):** We use conditional score-based diffusion models to calibrate simulator coefficients and residual fidelity domains sequentially based on newly collected online data, eliminating the need for full retraining.
- **Residual Fidelity:** To tackle the deficiency of the common simulator physics calibration, the proposed residual fidelity encompasses residual dynamics from simulation to the real world and residual environment from uncertain perceptions to simulation. Its diffusion model enables realistic environment generation, surpassing simple Gaussian noise, under the inferred distribution.
- **Informative Policy Adaptation:** We fine-tune the policy exclusively in anomalous situations. When NFC uncertainty is high and risks hindering policy improvement, we employ optimistic exploration under uncertainty to facilitate “hallucinated” policy optimization.

We systematically validate the effectiveness of our proposed NFC framework by comparing it with established methods for simulator parametric inference. Experiments on various sim-to-sim robots with high-dimensional parametric spaces demonstrate that NFC achieves superior inference and anomaly detection accuracy. Building on this algorithmic advantage, we evaluate the contribution of residual fidelity through simulated and real-world experiments. The results highlight the critical role of residual fidelity learning in improving policy perfor-

Y. Yu and L. Liu are with the Luddy School of Informatics, Computing, and Engineering at Indiana University, Bloomington, IN 47408, USA. E-mail: {youwyu, lantao}@iu.edu.

mance under challenging real-world conditions and anomalous scenarios.

II. RELATED WORK

In the realm of sim-to-real agile skill transfer, we first review progresses in robust behavior learning and focus on the adaptive domain randomization that calibrates the simulator to mirror the real-world environment. Then we discuss related works in how to fine-tune the RL policy with uncertain calibrations.

A. Robust Sim-to-Real Transfer

Zero-shot sim-to-real transfer with reinforcement learning has become prominent in agile locomotion [35, 87], navigation [41, 83], and dexterous manipulation [25, 80], where domain randomization is essential for bridging the sim-to-real gap. However, relying on repeated domain randomization alone can be inefficient and degrading robustness, prompting researchers to explore adversarial attacks and safe reinforcement learning.

Adversarial agents often enjoy privileges—such as applying destabilizing forces or altering physical parameters—to reveal policy vulnerabilities [59]. These agents may mimic normal agents while aiming to induce failures [19]. They can also be virtual adversaries that feed deceptive states to the agent, with vision-based inputs being especially susceptible [46]. [58] sampled worst-performing trajectories by tricking the agent into poor decisions, while [55] considered adversarial attacks under worst-case reward sequences. Moreover, the quadruped locomotion [66] used sequential attacks to show that domain randomization alone is insufficient against adversaries but can be fortified by adversarial training.

Safe reinforcement learning seeks to balance exploratory behavior with safety requirements. To achieve the constraints, constrained Markov decision processes incorporate risk measures such as CVaR [71], and Lagrangian methods transform constrained objectives into unconstrained ones [10]. Other approaches encode safety via Hamilton-Jacobi-Bellman-Isaacs variational inequalities [37] and control barrier functions [8]. Sim-Lab-Real [1] used Hamilton-Jacobi reachability to train a backup (safety) policy and probably approximately correct (PAC) Bayes framework to guarantee performance and safety. More recently, [54] proposed a predictive safety filter that simulates adversarial scenarios to preempt failures and ensure safe exploration. However, these methods cannot guarantee to handle all situations unless given sufficient simulation training, underscoring the need for continuous real-world adaptation without compromising safety.

B. Adaptive Domain Randomization

Adaptive domain randomization (ADR) aligns simulator parameters with real-world robot executions, providing insights into physical phenomena while narrowing the scope of domain randomization. Because of its theoretical generalizability, ADR has been applied to material cutting [29], soft robot

control [74], robot manipulation [38], and various simulated robot embodiments [60].

Most existing methods focus on improving the likelihood-free simulation-based inference (SBI) framework [57]. For instance, [60] used random Fourier features to highlight the sensitivity of approximate Bayesian computation (ABC) to distance metrics, and [53] introduced sequential inference for real-world scenarios, though the potential for high-dimensional time-series or image data [20] remains under-explored. [38] proposed differentiable causal factors to expose the sim-to-real gap. Under the family of information theory, [51] maximized Fisher information to identify trajectories highly sensitive to unknown parameters. Further, [43] integrated continual learning but only sampled randomization parameters in small subsets. Beyond inference-based methods, optimization techniques like evolution strategies [78], CMA-ES [74], and Bayesian optimization with Gaussian Processes [56] have also shown promise, albeit with higher computational costs. [61] highlighted the value of meta-learning [81] for further adaptation. Despite their general applicability, these methods still suffer from limited simulation budgets and mismatched simulation priors relative to real-world conditions.

Alternatively, optimization-based frameworks can bypass some of these constraints but often require differentiable simulators. For instance, a differentiable simulator for soft material cutting [29] achieved sharper inference via stochastic gradient Langevin dynamics (SGLD) compared to a non-differentiable approach [60], and [30, 31] demonstrated improvements with Stein variational gradient descent (SVGD) in manipulator mass inference. On one hand, these approaches often require extensive iterative simulations to achieve convergence. On the other hand, the idea of a perfectly calibrated simulator that precisely mirrors real-world dynamics remains elusive.

C. Optimistic Exploration under Uncertainty

A theoretically grounded approach to guide exploration, which has been extensively studied in single-agent RL, is the celebrated optimism in the face of uncertainty (OFU) principle. In a nutshell, it consists of choosing actions that maximize an optimistic estimate of the agent’s value function. OFU can efficiently balance exploration with exploitation and has been applied in several single-agent RL domains. R-Max [5] can be seen as an instance of a larger class of intrinsic reward based learning [2], but one where the reward is tied to state novelty. Hallucinated upper confidence reinforcement learning (H-UCRL) [12] modified the dynamics model with hallucinated controls to find the policy with greatest cumulative rewards under epistemic uncertainty. H-MARL [64] extended it to the multi-agent optimistic hallucinated game that seeks the coarse correlated equilibrium. On the other hand, [77] incorporated the information gain between the unknown dynamics and state observations to the optimal exploration objectives. With the dynamics model bootstrapped from model-based meta RL, H-URCL could guide exploration in an data effective fashion [3]. The regularization and epistemic uncertainty quantification were incorporated in both the meta-learning and task adap-

tation stages. Instead of pessimistic (safe) constraints that support only a subset of all possible valid plans, optimistic symbolic planner [70] allows for more plans than are possible in the true model.

III. PRELIMINARY

A. Simulator-Based Posterior Inference

Although domain randomization (DR) can mitigate the sim-to-real gap, it often requires expert knowledge of the real-world physics [48] or strategic adversarial attacks [66] to attain robust behavior. In comparison, the adaptive domain randomization [60] reasons the simulator controllable parameters ψ (e.g., friction, mass) from real-world experiences and iteratively “calibrate” the simulator via Bayesian inference $p(\psi|\tau) \propto p(\tau|\psi)p(\psi)$ with real-world trajectory τ . This approach narrows the DR space and can effectively promote the policy learning.

In this paper, we assume access to the black-box simulator that can investigate the dynamical system of any modeled robot embodiment. The simulator should be paralleable and run faster than wall-clock time. However, the main difficulty arises from the computation of likelihood $p(\tau^{\text{real}}|\psi)$. Among the likelihood-free inference approaches, the popular approximate Bayesian computation (ABC) sidesteps the previous problem. The basic rejection ABC approximates the posterior by $p(\|\tau^{\text{sim}}, \tau^{\text{real}}\| < \epsilon|\psi)$ with tolerance $\epsilon \geq \mathbf{0}$ using Monte Carlo simulations, where the choice of ϵ balances the accuracy and computation and can be improved through the sequential Monte Carlo (SMC-ABC [67]). Recently, ϵ -free ABC [57] approximates the posterior $\hat{p}(\psi|\tau) \propto \frac{p(\psi)}{\tilde{p}(\psi)}q(\psi|\tau)$ based on estimating Bayesian conditional density $q(\psi|\tau)$, where the proposal prior $\tilde{p}(\psi)$ describes the initial distribution of ψ . The process is iteratively trained until convergence. Although uniform distribution is a popular choice for $\tilde{p}(\cdot)$, in practice, ABC initialization demands heavy simulations that will delay the real-world online adaptation. On the other hand, as ψ conditions on the state and perception for mobile robots, vanilla deep learning methods can hardly outperform conditional diffusion models. The following section shows the idea of conditional diffusion models as neural posterior inference.

B. Neural Posterior Inference

Score-based diffusion models [69] are state-of-the-art generative methods based on stochastic differential equations (SDE). The forward diffusion process gradually adds noises to the original sample, denoted as $d\psi = \mathbf{f}(\psi, k)dk + g(k)d\mathbf{w}$ with time variable k , drift coefficient $\mathbf{f}(\cdot, k) : \mathbb{R}^d \rightarrow \mathbb{R}^d$, diffusion coefficient $g(\cdot) : \mathbb{R} \rightarrow \mathbb{R}$, and standard Wiener process \mathbf{w} . The score matching learns the dynamics of the reverse process, $d\psi = [\mathbf{f}(\psi, k) - g(k)^2 \nabla_{\psi} \log p_k(\psi|\tau)]dk + g(k)d\mathbf{w}$, where we condition the parameters ψ on robot trajectory τ . The conditional score matching for the neural posterior

inference [65] is trained via the following objective:

$$\psi^* = \underset{\psi}{\operatorname{argmin}} \mathbb{E}_k \left\{ \lambda(k) \mathbb{E}_{\psi(0)} \mathbb{E}_{\psi(k)|\psi(0)} \left[\left\| \mathbf{q}(\psi(k), \tau, k) - \nabla_{\psi(k)} \log p_{k|0}(\psi(k)|\psi(0)) \right\|_2^2 \right] \right\}. \quad (1)$$

To draw samples from $p(\psi|\tau^{\text{real}})$ with the executed trajectory, $\nabla_{\psi} \log p_k(\psi|\tau^{\text{real}}) \approx \mathbf{q}(\psi(k), \tau^{\text{real}}, k)$ simulates an approximation of the reverse diffusion process [65]. The neural posterior inference gains advantages over vanilla neural networks and kernel methods because of the success of diffusion generative methods family [33, 69].

C. Problem Formulation

The framework is modeled with contextual Markov decision processes [23], defined by the tuple $(\mathcal{S}, \mathcal{A}, r, \gamma, p, \mathcal{C})$, where \mathcal{S} is state space, \mathcal{A} is action space, $\gamma \in [0, 1)$ is discount factor, $r : \mathcal{S} \times \mathcal{A} \rightarrow \mathbb{R}$ is reward, and $p_c(\cdot|s, a)$ is dynamics with $c \in \mathcal{C}$, $s \in \mathcal{S}$, and $a \in \mathcal{A}$. The contextual space \mathcal{C} includes the simulated parameters ψ and environments (e.g., 3D geometry). We aim to optimize the policy $\pi : \mathcal{S} \rightarrow \mathcal{A}$ to efficiently tackle the unseen problems:

$$\min_{\psi} \mathcal{L}(\tau^{\text{real}}, \tau^{\text{sim}}) \quad \text{with} \quad \max_{\pi} \mathbb{E}_{s_{t+1} \sim p_c(s_{t+1}|s_t, a_t)} \left[\sum_{t=0}^T \gamma^t r(s_t, \pi(s_t)) \right] \quad (2)$$

where $\mathcal{L}(\tau^{\text{real}}, \tau^{\text{sim}})$ is distance metric.

Since the policy can be easily initialized in simulation, we will target informative policy fine-tuning during deployment. However, the objective $\min_{\psi} \mathcal{L}(\tau^{\text{real}}, \tau^{\text{sim}})$ may cause underestimation or over-fitting of τ , due to (1) the simulator can hardly replicate reality in all its details because of unmodeled dynamics factors, and (2) the dilemma of insufficient real-world observation and safety-critical robot executions. Although ABC has achieved notable successes in the single environment [60], its performance on mobile robots remains uncertain. As the simulator parameters ψ become more sophisticated, ABC may rely more heavily on the repeated simulation. In turn, the policy will be fine-tuned in a poorly calibrated simulator and execute uninformative and risky trajectory.

IV. METHOD

A. Neural Fidelity Calibration

The challenge is to efficiently calibrate the simulator parameters in simulation and mitigate the sim-to-real gap for training a resilient policy. Let ψ be the simulator controllable parameters, previous works based on Bayesian inference [60] gained successes with $p(\psi|\tau^{\text{sim}}) \propto p(\tau^{\text{sim}}|\psi)p(\psi)$ and the assumption $p(\psi|\tau^{\text{real}}) \propto p(\psi|\tau^{\text{sim}})$. However, even the most sophisticated simulator might not be able to represent reality in all its details, leading to poor estimation of $p(\psi|\tau^{\text{real}})$. Hence, we propose two distinct types of sim-to-real gaps - calibration and fidelity shifts.

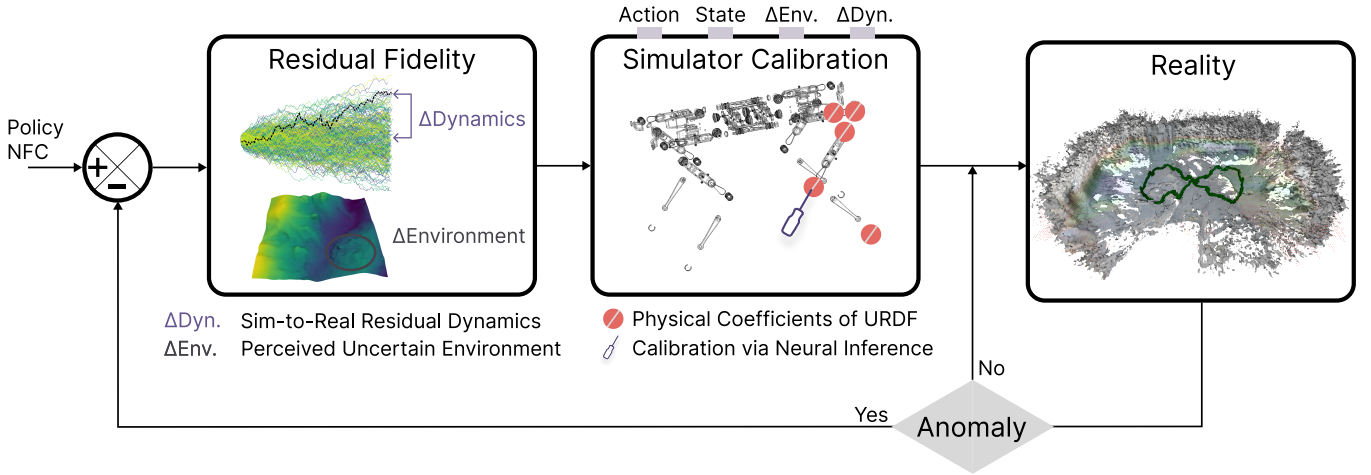


Fig. 1: Neural (diffusion-model) Fidelity (left-figure) Calibration (middle-figure), NFC, enables informative (anomaly-detection) sim-to-real (right-figure) policy transfer. Residual fidelity identifies dynamics shift from sim-to-real and residual environment from perception uncertainty. Simulator calibration finds suitable physical coefficients to match the real-world trajectory. In the left figure, colored trajectories represent those in the calibrated simulator, while the black trajectory corresponds to the real-world execution. The difference between them indicates the sim-to-real residual dynamics. The circled area on the elevated terrain highlights regions with uncertain perceptions, where our NFC samples the residual environment—the difference between the ground-truth terrain elevation and the perceived elevation—and reconstructs multiple terrain variations in simulation to fine-tune the policy. RL policy and NFC, initialized in simulation, are only fine-tuned under anomaly situations.

Definition 4.1 (Calibration and Fidelity Shifts). Calibration shifts signify that specific parameters are inadequately calibrated for simulating real-world scenarios, while fidelity shifts imply that certain modeling factors are overlooked in the abstract simulator.

$$s_{t+1} = \underbrace{f_{\psi}(s_t, a_t | e)}_{\text{Calibration}} + \underbrace{g_{\phi}(s_t, a_t | e)}_{\text{Fidelity}} + \epsilon(s_t, a_t | e). \quad (3)$$

This defines a general dynamics model incorporating simulator calibration parameters ψ , residual fidelity parameters $\phi = \{\Delta s, \Delta e\}$, state s_t , action a_t , environment e , and noise $\epsilon(\cdot)$. The function $f_{\psi}(\cdot)$ represents the black-box simulator, where inferring its physical parameters ψ reflects the calibration shift, aligning with the sim-to-real system identification task [39, 60]. The proposed residual fidelity model $g_{\phi}(\cdot)$ learns both the residual dynamics Δs capturing discrepancies between simulation and reality, and the residual environment Δe arising from uncertain onboard perceptions. The Bayesian inference of calibration and fidelity shifts is reformulated as follows:

$$p(\psi, \phi | \tau) \propto p(\tau | \psi, \phi) p(\psi, \phi), \quad (4)$$

where $\tau = \{(s_t, a_t)\}_{t=0}^H$ is the robot’s execution data in the real world by executing the policy $\pi(\cdot)$. Simulation-based inference is employed to infer the posterior distribution of the simulator parameter and residual fidelity models by minimizing the discrepancy between the real world and simulator. In Bayesian settings, minimizing this loss function translates to maximizing the posterior, which denotes our neural fidelity

calibrator as $q(\psi, \phi | \tau)$:

$$\begin{aligned} \mathcal{L}_{\text{Fidelity}} &= \min_{\psi, \phi} \mathcal{L}(\tau^{\text{real}}, \tau^{\text{sim}} | \theta) \\ \Rightarrow \psi^*, \phi^* &= \operatorname{argmax}_{\psi, \phi} \frac{1}{N} \sum_n \log q(\psi_n, \phi_n | \mathcal{F}_{\theta}(\tau_n)), \end{aligned} \quad (5)$$

where $\mathcal{L}(\cdot, \cdot)$ is a loss function measuring the discrepancy and $\mathcal{F}_{\theta}(\cdot)$ extracts the trajectory τ features. $q(\cdot, \cdot)$ is diffusion-based neural inference [65] with the posterior score:

$$\nabla_{\psi, \phi} \log p_k(\psi, \phi | \tau^{\text{real}}) \approx q(\psi(k), \phi(k), \tau^{\text{real}}, k), \quad (6)$$

where detailed $\mathcal{L}_{\text{Fidelity}}$ can be derived from Sec. III-B. To learn the representation $\mathcal{F}_{\theta}(\cdot)$ effectively, we propose to project the time series window into an embedding space with the casual temporal convolutional network [2]. The embedding space may contain multiple hyper-spheres [34], each representing different modes of the system’s behaviors. The training objective $f_{\psi}(s_t, a_t)$ also aligns with the privileged information reconstruction that has been proven effective in reducing the value discrepancy between the oracle and deployment policies [27].

Running Example. We have introduced the abstract concept of Neural Fidelity Calibration (NFC), which involves simulator calibration and residual fidelity shifts. To clarify its implementation, we illustrate it with a wheeled robot navigation scenario. Let the perceived environment be $e \in \mathbb{R}^{R \times C}$, representing a 3D elevation map obtained from depth sensors. The key parameters are defined as following:

- Simulator Calibration: $\psi \in \mathbb{R}^{17}$ represents physical parameters, including mass of the main body and four wheels $(\cdot) \in \mathbb{R}^5$, motor damping of four wheel joints $(\cdot) \in \mathbb{R}^4$, friction and restitution of four wheels $(\cdot) \in \mathbb{R}^8$.

- **Residual Fidelity:** $\phi = \{\Delta s, \Delta e\} \in \mathbb{R}^{15+R \times C}$ captures the residual dynamics $\Delta s_{t+1} = s_{t+1} - f_\psi(s_t, a_t) \in \mathbb{R}^{15}$ and the residual environment $\Delta e = \hat{e} - e \in \mathbb{R}^{R \times C}$. The dynamics model includes the orientation in quaternion ($\in \mathbb{R}^4$), linear velocity ($\in \mathbb{R}^3$), angular velocity ($\in \mathbb{R}^3$), position ($\in \mathbb{R}^3$), and previous action ($\in \mathbb{R}^2$). \hat{e} is the reconstructed environment in simulation.

Specifically, NFC conditions on the robot trajectory τ and perceived elevation map e , and outputs simulator parameters ψ and residual fidelity ϕ through a multi-head architecture, where three heads predict ψ , Δe , and Δs , respectively. In the simulator, we sample N pairs of physical coefficients ψ , residual dynamics Δs , and reconstructed environments $\hat{e} = e + \Delta e$. The physics engine $f_\psi(\cdot)$ then propagates the dynamics based on these sampled parameters.

B. Sequential Neural Fidelity Calibration

Another challenge lies in balancing data scarcity and robot safety. As the robot collects more data to refine NFC without policy fine-tuning, it faces increased risk. This necessitates iterative policy updates after each execution window. In the initial phase, the simulation-bootstrapped NFC provides an estimated proposal prior,

$$\tilde{p}(\psi, \phi) = \mathbf{q}(\psi, \phi | \tau^{\text{real}}), \quad (7)$$

which guides policy fine-tuning. This approach outperforms uniform priors and eliminates reliance on expert physics knowledge. For example, the state-of-the-art quadruped manipulation work [16] fused visual and tactile measurements to estimate ground friction¹.

Additionally, training diffusion models on large datasets is computationally demanding. Given a finite simulation budget, we adopt sequential NFC online, whose proposal posterior is:

$$\tilde{p}(\psi, \phi | \tau^{\text{real}}) = p(\psi, \phi | \tau^{\text{real}}) \frac{\tilde{p}(\psi, \phi) p(\tau^{\text{real}})}{p(\psi, \phi) \tilde{p}(\tau^{\text{real}})}, \quad (8)$$

where $p(\psi, \phi | \tau^{\text{real}})$ is the true posterior. This computationally efficient approach focuses on a narrower distribution and iterates until convergence, aligning with standard simulation-based calibration practices.

C. Neural Fidelity Randomization

As illustrated in the middle figure of the system overview in Fig.1, sampling calibrated simulator parameters ψ , such as friction and mass, is straightforward and computationally efficient. However, incorporating a perception module, essential for robotic applications [35, 52, 86, 87], introduces challenges in controlling randomness while preserving realism, particularly in geometry mapping.

Let the perceived environment be e . We redefine the robot execution τ as:

$$\tau = \{[s_t, a_t]_{t=0}^H, e_t\}, \quad (9)$$

¹While this could be integrated into NFC via Bayesian inference, we leave it for future work due to the requirement for a ground-truth multi-modal material dataset.

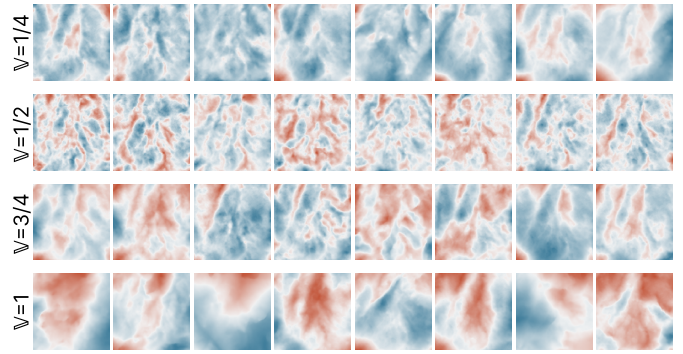


Fig. 2: Neural Fidelity Randomization enables sampling of high-dimensional residual environment geometries by accounting for perception uncertainty while preserving realism. As the (normalized) variance increases, the generated samples exhibit greater diversity in appearance.

where e_t represents the map constructed using depth sensors over a time window. In simulation, we sample various levels of depth sensor noise [24] and construct a dataset of noisy perception:

$$\Delta e = \hat{e} - \bar{e}, \quad (10)$$

where \bar{e} is the ground-truth environment. This approach generalizes to active sensors (e.g. LiDAR, Radar and depth cameras). During deployment, given the executed trajectory and perceived environment, $g\phi(\cdot, \cdot)$ samples residual environment and dynamics using diffusion-based neural inference [65]. While diffusion models can generate scene-scale geometries [42, 47, 83] and restore images [84], we focus on diffusion-based residual shifting for robot perception. Meanwhile, [84] supports our design choice of modeling residual environment rather than directly sampling the entire environment, reinforcing the efficiency and realism of our approach.

Running Example. Fig. 2 provides an example of the diffusion-sampled residual environment $\Delta e \in \mathbb{R}^{128 \times 128}$, where each pixel represents the elevation difference between simulated and perceived terrain. Although residual dynamics and simulator parameters are also sampled via diffusion, we omit their visualization as they resemble classic pseudo-random sampling. However, diffusion sampling is known to maintain realism and adhere to variance constraints [83].

In summary, our framework flexibly samples calibrated simulator parameters, residual environments, and dynamics, offering a principled approach to enhanced realism and adaptive learning.

V. INFORMATIVE SIM-TO-REAL ADAPTATION

To adapt the informative sim-to-real policy transfer, we fine-tune the policy only under anomalous situations, which are learned during the offline pretraining phase. Moreover, during the iterative loop of policy fine-tuning and neural fidelity calibration, a low-confidence belief initially can result in a wide posterior distribution, potentially degrading policy optimization. To mitigate this, we incorporate optimistic ex-

ploration under uncertainty, ensuring more effective policy adaptation.

A. Anomaly Detection

We propose a versatile robotic anomaly detection framework that integrates contrastive representation learning [9] with anomaly injection techniques [13]. To enhance detection accuracy, we utilize a historical context window alongside a detection target window, comparing their representations. A significant shift in the target window’s representation signals a potential anomaly in the system’s dynamics.

Our approach introduces Causal TCN $\mathcal{F}_\theta(\cdot)$, trained with a contrastive learning objective to map inputs from normal operational states onto a shared hypersphere [34]. The contrastive loss function maximizes similarity between the context τ^c and target τ^t windows under normal conditions while minimizing it during anomalies:

$$\mathcal{L}_{\text{Anomaly}}(\tau^c, \tau^t) = (\mathbb{1}_{c \neq t} - 1) \log[\text{loss}(\mathcal{F}_\theta(\tau^c), \mathcal{F}_\theta(\tau^t))] - \mathbb{1}_{c \neq t} \log[1 - \text{loss}(\mathcal{F}_\theta(\tau^c), \mathcal{F}_\theta(\tau^t))] \quad (11)$$

where $\mathbb{1}_{c \neq t}$ indicates an anomaly, $\mathcal{F}_\theta(\cdot)$ is the TCN encoder with parameters θ , $\text{loss}(\mathbf{a}, \mathbf{b}) = \exp[\cos(\mathbf{a}, \mathbf{b})/\lambda - 1]$ with temperature parameter $\lambda \geq 1$, and $\cos(\mathbf{a}, \mathbf{b}) := \langle \mathbf{a}, \mathbf{b} \rangle / (\|\mathbf{a}\| \|\mathbf{b}\|)$ measures the cosine similarity. Anomaly detection is inherently imbalanced, as real-world anomalies are scarce. To address this, we adopt anomaly injection strategies that disrupt temporal relations, introducing Global, Contextual, Seasonal, Shapelet, and Trend anomalies [13]. These techniques expand the model’s exposure to diverse anomalies, refining its decision boundary and improving robustness.

B. Policy Optimization with Hallucinated Randomness

Our proposed approach can be viewed as domain randomization with an inferred distribution over the randomization parameters (e.g., simulator physics, residual dynamics, and residual environment), which is an effective strategy for sim-to-real transfer when the inferred parameter posterior is precise. The policy is trained by maximizing the expected return with respect to the sampled transition function:

$$\pi^* = \underset{\pi}{\text{argmax}} \mathbb{E}_{s_{t+1} \sim p_{\psi, \phi}(s_{t+1} | s_t, a_t)} [R(\tau)], \quad (12)$$

where $r(\cdot)$ is the reward function, $p_{\psi, \phi}(x_{t+1} | x_t, u_t)$ describes the dynamics model, and we abbreviate the cumulative reward as $R(\tau) = \sum_{t=0}^T \gamma^t r(s_t, \pi(s_t))$. This greedy exploitation is widely used in model-based reinforcement learning [11, 14] to maximize expected performance. However, when posterior uncertainty is excessive, the sampled environments may negatively impact policy learning. For instance, sampling and fine-tuning in very low friction environments may cause the robot to slide uncontrollably, whereas high friction could result in it getting stuck. In both cases, the robot struggles to obtain reward signals within a short time, hindering effective online adaptation. To mitigate this issue, we propose granting the robot an uncertainty lever to control the randomness degree in its favor. Specifically, we introduce another unconditioned

policy $\pi_h(s_t)$, which we call the hallucinated policy, to modulate the uncertainty of the posterior distribution $p(\psi, \phi | \tau)$. The parameters are then sampled from a modified posterior distribution $p(\psi, \phi | \tau, \pi_h)$:

$$\psi, \phi \sim \mu(\psi, \phi) + \Sigma(\psi, \phi) \cdot \pi_h \quad (13)$$

with the mean $\mu(\psi, \phi)$ and variance $\Sigma(\psi, \phi)$ of $p(\psi, \phi | \tau)$.

This aligns with the principle of optimism in the face of uncertainty, proven effective for balancing exploration and exploitation [40], as well as enhancing data-efficient model-based reinforcement learning [12]. The policy learning problem is formulated as following:

$$\pi^*, \pi_h^* = \underset{\pi, \pi_h}{\text{argmax}} \mathbb{E}_{\hat{x}_t \sim p_{\psi, \phi, \pi_h}(x_t, u_t)} [R(\tau)], \quad (14)$$

which can be solved by policy optimization algorithms such as PPO [63].

C. Informative Sim-to-Real Adaptation with NFC

Algorithm 1 Informative Sim-to-Real Adaptation with NFC

Input: Initial policy π , simulator parameters ψ , residual fidelity ϕ , Neural Fidelity Calibration (NFC) $q(\psi, \phi | \cdot)$, anomaly detector, and hallucination policy π_h

Output: Optimized policy π^* , Dataset \mathcal{T}

Initialize: The policy π and NFC $q(\psi, \phi | \cdot)$ through simulation domain randomization training

- 1: **while** Mission not Complete **do**
 - 2: Execute trajectory τ_t
 - 3: **if** τ_t is anomalous **then**
 - 4: NFC $\psi, \phi \sim q(\psi, \phi | \tau)$ ▷ Eq. (4)
 - 5: Hallucinate $\psi, \phi \sim p(\psi, \phi | \tau, \pi_h)$ ▷ Eq. (13)
 - 6: Sample $\{\psi\}^N, \{\phi = [\Delta e, \Delta s]\}^N$
 - 7: $\pi', \pi_h' = \text{Policy-Opt}(\pi, \pi_h, \psi, \phi)$ ▷ Eq. (14)
 - 8: $q(\cdot) \leftarrow q(\{\psi\}^N, \{\phi\}^N | \{\tau\}^N)$ ▷ Sequential NFC
 - 9: **end if**
 - 10: $\mathcal{T} = \mathcal{T} \cup \tau_t, t \leftarrow t + 1$ ▷ Update Dataset
 - 11: **end while**
 - 12: Fine-tune NFC and Anomaly Detector with \mathcal{T}
-

We summarize our framework in Algorithm 1, where an SDE-based diffusion model samples residual dynamics Δs and residual environment Δe . The overall process consists of three main stages. First, in simulation pretraining, we bootstrap both the RL policy π and Neural Fidelity Calibration (NFC) $q(\psi, \phi | \cdot)$ using a uniform domain randomization strategy. This phase is general and follows domain randomization [48] with teacher-student distillation [7], ensuring a broad initial policy and NFC prior. Second, during real-world deployment, we fine-tune the policy only under anomalous situations. Unlike robot information gathering (RIG) [36], which actively seeks phenomenon of interest, our primary focus is mission execution. In fact, our framework can be viewed as a mission-oriented search, where the mission can involve RIG or sequential goal-reaching tasks. This flexibility allows NFC to be

seamlessly integrated into RIG for further exploration when needed. Third, to improve efficiency, we build a sequential NFC online that leverages the proposal prior from the offline pretrained NFC. This allows the model to adapt using only online data, reducing the need for extensive retraining. After completing the mission, the collected physical and residual fidelity knowledge is used to fine-tune the original NFC, further refining the sim-to-real adaptation. This structured approach ensures efficient learning, minimizes unnecessary retraining, and maintains robust real-world performance under uncertain and anomalous conditions.

VI. SIMULATION EXPERIMENT

We first evaluate anomaly detection and simulator parametric calibration through sim-to-sim experiments across diverse robotic embodiments, comparing our NFC with competing baselines. Building on these algorithmic results, we assess policy fine-tuning performance, comparing NFC with an online model-based RL method. Additionally, we ablate the impact of Residual Fidelity on flat and unstructured environments. The sim-to-sim experiments aim to address the following research questions:

- Anomaly Detection Accuracy: How well does our TCN-based anomaly detection generalize across different robot platforms?
- NFC Performance: How effectively do our SDE-Diffusion and TCN-based NFC calibrate simulator physical parameters and residual fidelity, compared to state-of-the-art methods across multiple robot platforms?
- Policy Fine-Tuning and Residual Fidelity Contribution: If NFC outperforms competing methods, to what extent does it enhance policy fine-tuning, and what is the impact of the Residual Fidelity module?

A. Sim-to-Sim Experiment Settings

We evaluate on standard benchmark robots with a focus on mobile embodiments. Various robots, including *Ant*, *Quadruped*, *Humanoid*, *Quadcopter*, and *Jackal*, are trained in IsaacGym [49] and evaluated in Mujoco simulator [76]. The ClearPath *Jackal*, a compact differential-wheeled robot with a low chassis, presents a challenge for controller robustness. During offline learning, all robots follow a similar training structure as quadruped locomotion [52], using PPO [62]. Each robot is equipped with a depth camera, modeled after the RealSense D435, to construct elevation maps [17]. In IsaacGym, we parallelize 100 environments, each containing 100 robots, collecting 10^6 episodes for policy and NFC initialization. An episode consists of recorded actions and states from start to end. During online inference, Mujoco runs one episode per iteration to mirror the real-world evaluation. Both simulators operate at 200 Hz, with policies executing at 50 Hz.

The simulator physical coefficients ψ primarily consist of mass, friction, and stiffness for the robot’s joints and links. Across *Ant*, *Quadruped*, *Humanoid*, *Quadcopter*, and *Jackal*, the dimensions of ψ are $\{21, 13, 37, 9, 17\}$, while

the trajectory window H has dimensions $\{50, 20, 20, 20, 50\}$, with detailed settings provided in Appendix B. The residual fidelity $\phi = \{\Delta e, \Delta s\}$ includes residual ego-centric geometry $\Delta e \in \mathbb{R}^{128 \times 128}$ with a resolution of 0.1 m and residual dynamics Δs with dimensions $\{52, 48, 21, 108, 15\}$, where Δe represents the difference in environment elevations between the simulated and perceived terrain.

We conduct experiments in both *Flat* and *Rough* environments while introducing Gaussian noise in Mujoco to the robot state, perception, and motor control. *Flat* corresponds to a simulated empty world without obstacles, whereas *Rough* consists of unstructured environments, where *Quadcopter* navigates randomized 3D obstacle environments [44] and ground robots traverse randomized elevated terrains [83].

B. Baselines and Ablations

We evaluate the effectiveness of our causal temporal convolutional network (TCN) against vanilla neural networks (NN), quasi-Monte Carlo random Fourier features (QMC-RFF), and quasi-Monte Carlo fast kernel slicing (QMC-FKS) based on the non-equispaced fast Fourier transform. Here, QMC refers to quasi-Monte Carlo sampling using the Sobol sequence. For fairness, all kernel-based methods use the same Gaussian basis function for kernels, with 1024 features, and an equivalent last-layer size for NN and TCN. Consistently, we employ the score-based diffusion model (SDE) [65] for neural posterior inference. We also include the state-of-the-art ϵ -free method [60], which employs a mixture density network (MDN) [4] combined with QMC-RFF. For experimental completeness, we evaluate MDN with TCN to assess its performance in comparison to other approaches. Notably, kernel methods do not account for environment perception, whereas TCN and NN explicitly incorporate it.

To justify kernel choices, RFF approximates the radial basis function (RBF) for computational efficiency in high-dimensional settings and has empirically outperformed NN [60]. FKS, on the other hand, offers theoretical advantages over RFF: Bochner’s theorem does not hold for conditionally positive definite kernels, meaning RFF may over-smooth non-smooth kernels. Details on RFF and our FKS implementation [32] are provided in Appendix A3.

C. Anomaly Detection Results

After pretraining in IsaacGym, robots are deployed in Mujoco, where we randomly inject anomalous values into simulator physical parameters and fidelity domains. These anomalies consist of values out of distribution to the offline pretraining. Since policy improvement relies on successful anomaly detection and neural fidelity inference, we evaluate their performance through extensive simulations in this section and the next.

For each method in each scenario, we use 10^6 offline training samples. NN and TCN are conditioned on both the robot trajectory and perception. Kernel methods, however, only have access to the robot trajectory. During Mujoco deployment, we sample 2×10^4 data points for anomaly detection, though only

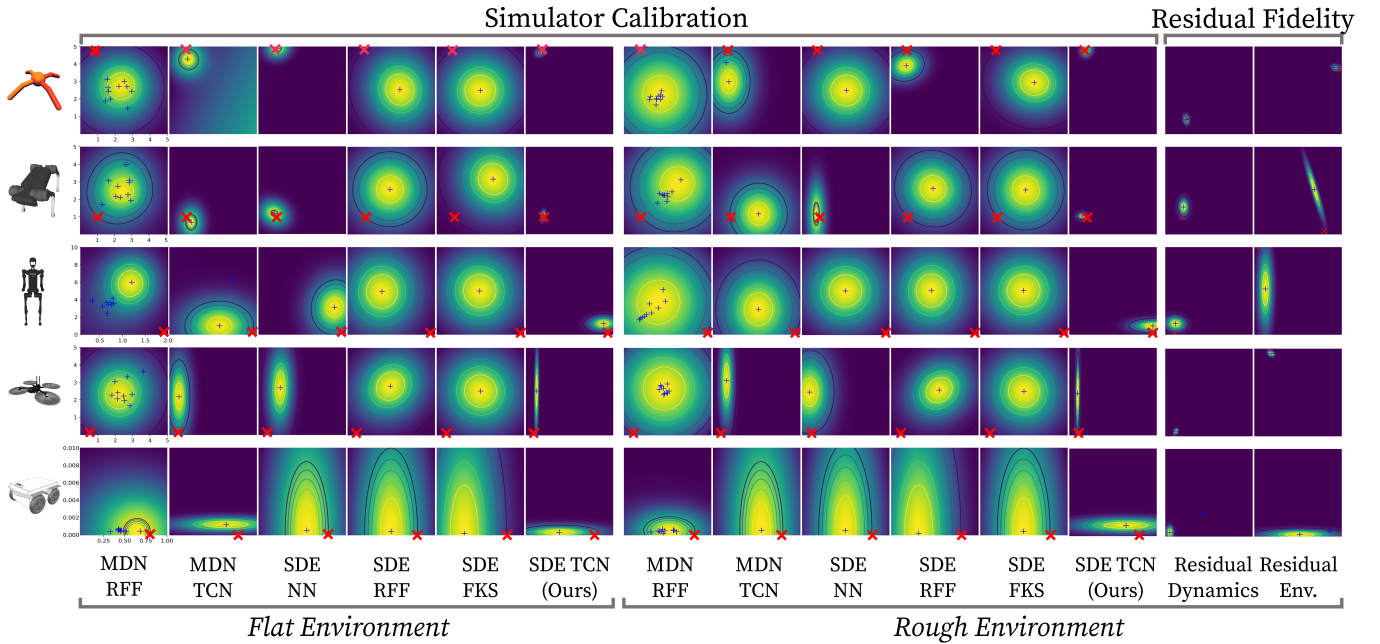


Fig. 3: Simulator calibration posterior across five robots is compared between our method and competing approaches in *Flat* (empty-world) and *Rough* (unstructured) environments, with the ground-truth values marked by red crosses. The residual fidelity posterior, which includes residual dynamics (position x and y) and residual environment (height in z), is only shown for our method due to the poor performance of other approaches. Simulator calibration parameters: [Ant] torso mass v.s. left back foot mass, [Quadruped] rear front shank mass v.s. right rear shank mass, [Humanoid] torso mass v.s. right hip stiffness, [Quadcopter] first rotor mass v.s. rotor third arm mass, [Jackal] rear right wheel damping v.s. front left wheel restitution.

Inference	Feature	Average Logarithm Posterior of Simulator Calibration Parameters \uparrow										Anomaly Detection			
		Ant		Quadruped		Humanoid		Quadcopter		Jackal		TPR \uparrow		FPR \downarrow	
		<i>Flat</i>	<i>Rough</i>	<i>Flat</i>	<i>Rough</i>	<i>Flat</i>	<i>Rough</i>	<i>Flat</i>	<i>Rough</i>	<i>Flat</i>	<i>Rough</i>	<i>Flat</i>	<i>Rough</i>	<i>Flat</i>	<i>Rough</i>
MDN	QMC-RFF	-4.88	-0.59	-2.09	-2.3	-10.52	-13.27	-2.26	-2.47	0.64	-1.2	1	0.96	0.3	0.33
MDN	TCN	-2.6	-3.1	-1.64	-3.11	-2.52	-3.42	-1.79	-2.56	0.22	-1.17	1	1	0	0
SDE	NN	-1	-1.09	-1.14	-1.34	-1.63	-2.93	-1.2	-1.86	0.26	-1.1	1	1	0	0
SDE	QMC-RFF	-2.79	-3.03	-2.17	-2.48	-2.61	-3.33	-3	-3.64	0.06	-1.29	1	0.96	0.3	0.33
SDE	QMC-FKS	-2.63	-3.05	-2	-1.91	-2.41	-3.37	-2.42	-2.73	0.24	-1.16	1	0.97	0	0
SDE	TCN (Ours)	0.57	0.46	-0.42	-0.46	-1.03	-2.64	-0.9	-1.5	1.21	0.69	1	1	0	0

TABLE I: Statistical results for anomaly detection among different features. Five different robots on *Flat* (empty world) and *Rough* (unstructured) environments demonstrate the importance and affect of perception on anomaly detection performance.

one is used for policy improvement. Among these samples, 10^4 are anomalous (true positives), while the remaining 10^4 are normal (false positives). Table I reports the true positive rate (TPR) and false positive rate (FPR). Since our focus is on feature representations rather than theoretical advancements in anomaly detection, we provide a summary of results. As shown in Table I, our TCN achieves the highest TPR and lowest FPR across all robots on both scenarios. Additionally, since TPR and FPR testing use an equal number of samples, our method also attains the best precision, demonstrating its superior ability to distinguish anomalies. Moreover, the results of anomaly detection and simulator calibration are inherently connected rather than disjoint. In the following section, we shift our focus to the more critical aspect of simulator calibration.

D. Neural Fidelity Calibration Results

More importantly, Fig. 3 illustrates posterior inference across five robot embodiments, where we randomly select two domains' joint posterior per robot due to space constraints. Table I reports the average log posterior of simulator calibration parameters, while the right side of Fig. 3 presents the residual fidelity results, including residual dynamics and residual environment, inferred by our NFC. The displayed residual dynamics consists of residual position in x and y , while the residual environment consists of residual height in z . We exclude other methods from residual fidelity evaluation, as kernel-based approaches struggle with high-dimensional data, and vanilla NN performs worse than diffusion models.

For simulator calibration, recall that physical coefficient dimensions are $\{21, 13, 37, 9, 17\}$. All baseline methods exhibit poor inference accuracy due to the high-dimensional input-output space, whereas our NFC (SDE with TCN) consistently

outperforms them on both selected domains and average results. Performance drops from *Flat* to *Rough* environments and across robot complexity from Ant to Quadruped to Humanoid, highlighting the challenge of Bayesian inference in high-dimensional spaces (input dimension > 4096). Moreover, our neural inference with **SDE-Diffusion** surpasses **MDN** in both RFF kernel and TCN encoder, further demonstrating the advantage of diffusion models over vanilla NNs. Given these results, we consistently use **NFC** for policy fine-tuning in subsequent experiments.

For residual fidelity, Fig. 3 shows strong inference performance of **NFC** for residual dynamics and residual environment, though the latter poses a greater challenge due to its higher dimensionality. This aligns with the broader difficulty of learning accurate posteriors in high-dimensional spaces. The next section further explores residual fidelity’s contribution to policy improvement. Here, we do not include other methods, as kernel-based approaches struggle with high-dimensional spaces, and NN generally underperform compared to diffusion models in high-dimensional generation tasks.

A potential controversy arises regarding NN’s size. Increasing the multi-layer perceptron (MLP) size to 256 times the default configuration in [60] allows NN to surpass **RFF**. While larger NN may outperform other methods, our focus remains on precise inference with real-time performance. Future research will explore alternative architectures, such as Transformers [79], to further improve inference quality.

E. Policy Improvement Results

This section evaluates policy improvement with our neural fidelity calibration (**NFC**). Based on **NFC** performance in the previous anomaly detection and fidelity calibration experiments, we benchmark our **PPO w/ NFC** and ablate the Residual Fidelity module (**PPO w/o Δ Fidelity**) to assess its impact. Experiments in *Flat* and *Rough* environments further validate the contribution of Residual Fidelity. Additionally, we ablate **NFC** entirely by fine-tuning the PPO policy directly on online execution data, denoted as **PPO w/o NFC**. To extend the comparison, we include an explicit model-based reinforcement learning (MBRL) algorithm, **TD-MPC2** [26], which is co-pretrained with PPO and directly fine-tunes the dynamics model from real-world robot trajectories. We choose TD-MPC2 due to its superior data efficiency compared to model-free RL (e.g., PPO [62], SAC [21]) and even other model-based RL algorithms (e.g., DreamerV3 [22]). Note that we do not explore alternative exploration strategies, such as greedy exploration or Thompson sampling, as the effectiveness of the hallucinated policy has already been extensively studied [12, 50, 73].

Table II presents the sim-to-sim policy improvement results across five different robots, comparing four methods. The average return, computed as the cumulative reward, is normalized to $[0, 1]$ using the running maximum and minimum values. Our approach, **PPO w/ NFC**, consistently achieves the best performance on the Mujoco testing platform. The results highlight the importance of neural fidelity, as performance

Average Return $[0, 1]$		PPO	PPO	PPO	TD-MPC2
		w/ NFC	w/o Δ Fidelity	w/o NFC	
Ant	<i>Flat</i>	0.98	0.88	0.64	0.87
	<i>Rough</i>	0.95	0.81	0.57	0.75
Quadruped	<i>Flat</i>	0.67	0.33	0.17	0.42
	<i>Rough</i>	0.55	0.27	0.18	0.18
Humanoid	<i>Flat</i>	0.96	0.89	0.55	0.88
	<i>Rough</i>	0.93	0.9	0.58	0.88
Quadcopter	<i>Flat</i>	0.82	0.75	0.67	0.72
	<i>Rough</i>	0.81	0.69	0.33	0.67
Jackal	<i>Flat</i>	0.87	0.67	0.23	0.41
	<i>Rough</i>	0.82	0.69	0.2	0.41

TABLE II: Statistical results for policy improvement among our method PPO w/ NFC, the ablations, and TD-MPC2. Five different robots on *Flat* (empty-world) and *Rough* (unstructured) environments demonstrate the importance and affect of residual fidelity on policy fine-tuning performance.



Fig. 4: Real-world experiment environments with various surfaces and physical properties. The vehicle’s left front axle was broken as an anomalous situation, whereas the additional rock posed challenging inertia force.

consistently drops when the neural fidelity module is ablated (PPO w/o Δ Fidelity). Furthermore, removing the entire **NFC** module (PPO w/o **NFC**) results in a significant performance drop, emphasizing how **NFC** refines the domain randomization range for more effective adaptation.

TD-MPC2, fine-tuned online using only robot execution data, benefits from the sample efficiency of model-based RL across all robots and environments. It outperforms PPO w/o **NFC** but not PPO w/o Δ Fidelity, even with limited online data. However, due to the constraints of onboard computation, real-time execution remains a challenge for model-based RL. While PPO w/ **NFC** operates at 25 Hz, TD-MPC2 can only achieve 6 Hz, making it impractical for real-time control in many robotic applications.

VII. REAL-WORLD IMPLEMENTATION

We implement our framework on the differential drive robot, ClearPath Jackal, operating under challenging anomalous conditions. To extend our simulation experiments, we evaluate the robot in environments ranging from *Flat* (laboratory surfaces) to *Rough* (wild terrains). This section highlights the challenges associated with real-world computation and deployment.

A. Experimental Settings

The robot is equipped with a RealSense D435i camera, a 16-beam Velodyne LiDAR, and a MicroStrain 3DM-GX5-25 IMU. The depth camera (30 Hz) and LiDAR-inertial odometry (200 Hz) provide real-time elevation mapping [17] on GPU. Onboard computation uses an NVIDIA Jetson Orin and offboard policy optimization uses an NVIDIA RTX3080Ti Mobile GPU. Fig. 4 illustrates the experimental environments, covering a range of laboratory surfaces and wild elevated terrains with complex physical properties. We evaluate two anomalous situations: (1) A broken front left wheel axle, and (2) A broken front left wheel axle with an added rock (not tightly attached). The rock is included only in lab environments, as its mass and inertia introduce significant challenges even for flat-surface navigation.

Specifically, as shown in Fig. 4, *Flat* represents the lab environment, where we evaluate three conditions: (1) a broken front left wheel axle, (2) a broken front left wheel axle with an added rock (not tightly attached), and (3) a broken front left wheel axle with an added rock on surfaces with different materials. *Rough* represents wild terrains, including snowy, muddy, wet grass, and elevated surfaces, all tested with a broken front left wheel axle. The rock is not included in these environments, as it would likely make the mission impossible to complete. In each environment, the controller is tasked with following a figure-8 trajectory with a 3 m diameter. Each controller is tested 9 times in each scenario.

Our method is employed for anomaly detection, achieving a 100% success rate. Following a similar procedure as in the simulated experiments, we compare *NFC* (SDE with TCN) against *NN*, *RFF*, *FKS*, and *MDN* for the simulator parametric calibration comparison. For policy improvement, we evaluate *PPO w/ NFC* alongside its ablations, *PPO w/o NFC* and *PPO w/o ΔFidelity*, as well as the model-based reinforcement learning method *TD-MPC2*, which only fine-tunes with the online robot execution data. Additionally, we include a motion primitive planner, *Falco* [85], which is widely recognized for its real-time performance and generalizability [6, 82]. *Falco* uses Dubins dynamics and employs a well-tuned PID controller running at 200 Hz.

B. Neural Fidelity Calibration Results

We present the comparison of simulator calibration and the results of our residual fidelity in Fig. 6. The calibration of the front left wheel’s damping averages at 0, while the friction across all four wheels averages at 0.4, reflecting the broken front left wheel axle on snowy terrains. Competing methods, despite being trained on the same dataset, perform poorly across all domains. This result aligns with our sim-to-sim experiments, reinforcing our method’s superiority in high-dimensional parameter spaces. We also present the results of the residual fidelity module, with residual dynamics shown in Fig. 6 and residual environment in Fig. 5. However, since the ground-truth distribution of residual dynamics and residual environment is unavailable, we further evaluate its impact on policy improvement in the next section.

C. Policy Improvement Results

		PPO w/ NFC	PPO w/o ΔFidelity	PPO w/o NFC	TD-MPC2	Falco
Success Rate (%)	<i>Flat</i>	100	100	100	100	100
	<i>Rough</i>	72	53	25	42	28
Traj. Ratio	<i>Flat</i>	1.8	1.8	1.9	1.5	1.6
	<i>Rough</i>	2.1	3.2	3.7	2.7	3.6
Orien. Jerk (rad/s ³)	<i>Flat</i>	2.98	3.5	14.18	6.95	41.9
	<i>Rough</i>	3.19	8.49	26.99	8.98	41.93
Pos. Jerk (m/s ³)	<i>Flat</i>	4.36	9.32	8.41	5.27	6.95
	<i>Rough</i>	6.26	12.46	12.42	18.46	8.87

TABLE III: Statistical results for policy improvement among our method *PPO w/ NFC*, the ablations, and *TD-MPC2*. Five different robots on *Flat* (empty-world) and *Rough* (unstructured) environments demonstrate the importance and affect of residual fidelity on anomaly policy fine-tuning performance.

As shown in Table III, the real-world scenarios pose great challenges to the wheeled robot. We decompose the analysis into three parts, including the contribution of our *NFC*, the ablation of our Residual Fidelity, and the baselines. We follow previous works [68, 83] and evaluate performance using success rate, trajectory ratio, orientation jerk $\left| \frac{\partial^2 \omega}{\partial t^2} \right|$, and position jerk $\left| \frac{\partial a}{\partial t} \right|$, where ω and a represent angular velocity and linear acceleration, respectively. These motion stability indicators are critical for reducing sudden pose changes and enhancing

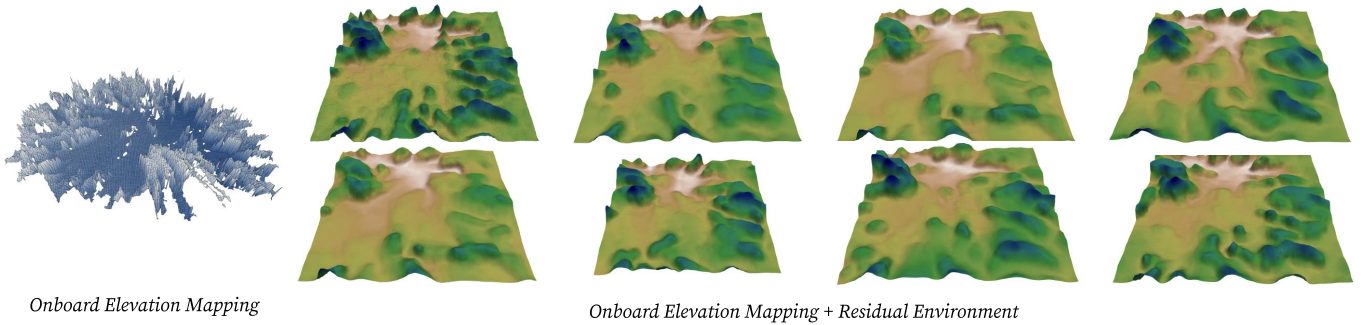


Fig. 5: Our Neural Fidelity infers the residual environment $\{\Delta e\}^N$ based on the uncertain onboard elevation mapping e in the real world. The right side shows $N = 8$ reconstructed environments, $\hat{e} = e + \Delta e$, in simulation to fine-tune the policy.

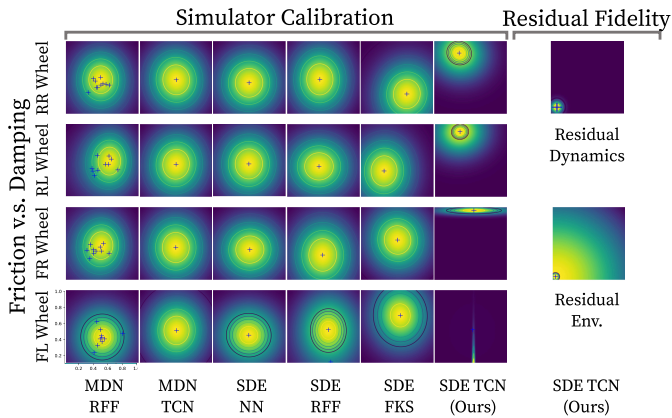


Fig. 6: Neural Fidelity Calibration results of wheeled robot navigating real-world snowy surfaces, with the front left wheel axle broken.

overall safety. The trajectory ratio, defined as the successful path length relative to the straight-line distance, serves as a measure of navigator efficiency.

First, the contribution of NFC to online policy improvement is crucial. When NFC is ablated and the policy is fine-tuned using only the perceived data, PPO shows minimal improvement across all environments. While PPO still achieves a 100% success rate in the *Flat* environment, it records low performance across all metrics. During policy deployment, we observe frequent jerks caused by PPO w/o NFC, which the policy was not trained to handle. This issue worsens in wild environments, where the policy exhibits repetitive back-and-forth movements with harsh jerks, indicating it fails to find a viable solution to the goal and is likely stuck in local minima. One notable deficiency of our NFC occurs in the *Flat* environment. Although the fine-tuned policy learns to navigate under anomalous conditions, its trajectory ratio metric remains unsatisfactory. A potential reason for this is the lack of trajectory length penalization in the reward function, which we will address in future research to improve the overall performance.

Second, we examine the contribution of Residual Fidelity in NFC to online policy improvement. Fig. 5 illustrates the onboard perceived environment, which is noisy, incomplete, and deceptive due to complex geometry, lighting variations, and material properties in the wild environment. One potential approach is to directly use the perceived map and apply numerical interpolation to fill in missing data in simulation. However, PPO w/o Δ Fidelity shows little improvement over PPO w/o NFC, and it cannot outperform TD-MPC2 in all metrics. On one hand, PPO w/o Residual Fidelity does not exhibit frequent jerks like PPO w/o NFC, as it still benefits from simulator calibration fine-tuning. On the other hand, its performance remains inferior, as it fails to adapt to the noisy dynamics and perception uncertainties present in the real-world deployment.

Third, the classic method Falco achieves good position jerk statistics due to its high control rate. TD-MPC2, which is

fine-tuned using only online execution data, also demonstrates advantages over PPO w/o NFC. As observed in the sim-to-sim experiments, TD-MPC2 benefits from the sample efficiency of model-based RL but suffers from computational inefficiencies, especially when incorporating perception into state propagation. The results further highlight the importance of our NFC module. Initially, PPO alone does not outperform TD-MPC2, but after fine-tuning with NFC, PPO significantly surpasses TD-MPC2, demonstrating the effectiveness of NFC-driven policy adaptation in real-world environments.

In summary, our NFC module significantly enhances policy improvement in the challenging navigation task, effectively handling both a broken wheel axle and diverse, complex environments.

VIII. CONCLUSION, LIMITATIONS AND FUTURE DIRECTIONS

We propose Neural Fidelity Calibration (NFC) to simultaneously calibrate simulator physics and residual fidelity parameters, facilitating policy fine-tuning online. Our novel residual fidelity consists of residual dynamics and residual environment, where the former captures the simulation shift relative to real-world dynamics and the latter quantifies uncertainty in environmental perception. Leveraging NFC’s superior posterior inference, we enhance real-world adaptability by integrating anomaly detection, sequential NFC, and optimistic exploration. Extensive sim-to-sim and sim-to-real experiments validate NFC’s effectiveness, demonstrating its critical role in policy improvement and its superiority over both classic and learning-based approaches.

Limitations and Future Directions. While our approach assumes a black-box simulator, estimating the gradient of robot trajectories w.r.t. physical coefficients and residual fidelity factors using perturbation theory could significantly accelerate inference. The emergence of general and differentiable simulators further presents an opportunity to expedite solutions. Another potential enhancement involves incorporating multi-modal information, such as image segmentation, but this raises the question of whether decomposing conditions would allow greater flexibility across different perception modules. This also assumes independent and identically distributed conditions across different perception modules, which may not hold in real-world scenarios. Finally, we aim to explore model-based reinforcement learning to learn a residual controller model, integrating it with NFC to build a more explainable and structured framework.

REFERENCES

- [1] [Sim-to-Lab-to-Real: Safe reinforcement learning with shielding and generalization guarantees](#). *Artificial Intelligence*, 314:103811, 2023. ISSN 0004-3702.
- [2] Shaojie Bai, J. Zico Kolter, and Vladlen Koltun. [An Empirical Evaluation of Generic Convolutional and Recurrent Networks for Sequence Modeling](#). *arXiv:1803.01271*, 2018.

- [3] Arjun Bhardwaj, Jonas Rothfuss, Bhavya Sukhija, Yarden As, Marco Hutter, Stelian Coros, and Andreas Krause. [Data-Efficient Task Generalization via Probabilistic Model-Based Meta Reinforcement Learning](#). *IEEE Robotics and Automation Letters*, 9(4):3918–3925, 2024.
- [4] Christopher M Bishop. [Mixture density networks](#). 1994.
- [5] Ronen I Brafman and Moshe Tennenholtz. [R-max—a general polynomial time algorithm for near-optimal reinforcement learning](#). *Journal of Machine Learning Research*, 3(Oct):213–231, 2002.
- [6] C. Cao, H. Zhu, Z. Ren, H. Choset, and J. Zhang. [Representation granularity enables time-efficient autonomous exploration in large, complex worlds](#). *Science Robotics*, 8(80):eadf0970, 2023.
- [7] Dian Chen, Brady Zhou, Vladlen Koltun, and Philipp Krähenbühl. [Learning by Cheating](#). In Leslie Pack Kaelbling, Danica Kragic, and Komei Sugiura, editors, *Proceedings of the Conference on Robot Learning*, volume 100 of *Proceedings of Machine Learning Research*, pages 66–75. PMLR, 30 Oct–01 Nov 2020.
- [8] Richard Cheng, Gábor Orosz, Richard M. Murray, and Joel W. Burdick. [End-to-end safe reinforcement learning through barrier functions for safety-critical continuous control tasks](#). *AAAI’19/IAAI’19/EAAI’19*. AAAI Press, 2019. ISBN 978-1-57735-809-1.
- [9] Sumit Chopra, Raia Hadsell, and Yann LeCun. [Learning a similarity metric discriminatively, with application to face verification](#). In *2005 IEEE computer society conference on computer vision and pattern recognition (CVPR’05)*, volume 1, pages 539–546. IEEE, 2005.
- [10] Yinlam Chow, Mohammad Ghavamzadeh, Lucas Janson, and Marco Pavone. [Risk-Constrained Reinforcement Learning with Percentile Risk Criteria](#). *Journal of Machine Learning Research*, 18(167):1–51, 2018.
- [11] Kurtland Chua, Roberto Calandra, Rowan McAllister, and Sergey Levine. [Deep reinforcement learning in a handful of trials using probabilistic dynamics models](#). *Advances in neural information processing systems*, 31, 2018.
- [12] Sebastian Curi, Felix Berkenkamp, and Andreas Krause. [Efficient model-based reinforcement learning through optimistic policy search and planning](#). *Advances in Neural Information Processing Systems*, 33:14156–14170, 2020.
- [13] Zahra Zamanzadeh Darban, Geoffrey I Webb, Shirui Pan, Charu C Aggarwal, and Mahsa Salehi. [CARLA: Self-supervised contrastive representation learning for time series anomaly detection](#). *Pattern Recognition*, 157: 110874, 2025.
- [14] Marc Deisenroth and Carl E Rasmussen. [PILCO: A model-based and data-efficient approach to policy search](#). In *Proceedings of the 28th International Conference on machine learning (ICML-11)*, pages 465–472, 2011.
- [15] Alejandro Escontrela, Justin Kerr, Kyle Stachowicz, and Pieter Abbeel. [Learning Robotic Locomotion Affordances and Photorealistic Simulators from Human-Captured Data](#). In *8th Annual Conference on Robot Learning*, 2024.
- [16] Parker Ewen, Hao Chen, Yuzhen Chen, Anran Li, Anup Bagali, Gitesh Gunjal, and Ram Vasudevan. [You’ve Got to Feel It To Believe It: Multi-Modal Bayesian Inference for Semantic and Property Prediction](#). In *Proceedings of Robotics: Science and Systems*, Delft, Netherlands, July 2024.
- [17] Péter Fankhauser, Michael Bloesch, and Marco Hutter. [Probabilistic Terrain Mapping for Mobile Robots with Uncertain Localization](#). *IEEE Robotics & Automation Letters*, 3(4):3019–3026, 2018.
- [18] Ismail Geles, Leonard Bauersfeld, Angel Romero, Jiaxu Xing, and Davide Scaramuzza. [Demonstrating Agile Flight from Pixels without State Estimation](#). In *Proceedings of Robotics: Science and Systems*, Delft, Netherlands, July 2024.
- [19] Adam Gleave, Michael Dennis, Cody Wild, Neel Kant, Sergey Levine, and Stuart Russell. [Adversarial Policies: Attacking Deep Reinforcement Learning](#). In *International Conference on Learning Representations*, 2020.
- [20] David Greenberg, Marcel Nonnenmacher, and Jakob Macke. [Automatic posterior transformation for likelihood-free inference](#). In *International Conference on Machine Learning*, pages 2404–2414. PMLR, 2019.
- [21] Tuomas Haarnoja, Aurick Zhou, Pieter Abbeel, and Sergey Levine. [Soft actor-critic: Off-policy maximum entropy deep reinforcement learning with a stochastic actor](#). In *International conference on machine learning*, pages 1861–1870. PMLR, 2018.
- [22] Danijar Hafner, Jurgis Pasukonis, Jimmy Ba, and Timothy Lillicrap. [Mastering diverse domains through world models](#). *arXiv preprint arXiv:2301.04104*, 2023.
- [23] Assaf Hallak, Dotan Di Castro, and Shie Mannor. [Contextual Markov Decision Processes](#), 2015.
- [24] Georg Halmetschlager-Funek, Markus Suchi, Martin Kampel, and Markus Vincze. [An Empirical Evaluation of Ten Depth Cameras: Bias, Precision, Lateral Noise, Different Lighting Conditions and Materials, and Multiple Sensor Setups in Indoor Environments](#). *IEEE Robotics & Automation Magazine*, 26(1):67–77, 2019.
- [25] Ankur Handa, Arthur Allshire, Viktor Makoviychuk, Aleksei Petrenko, Ritvik Singh, Jingzhou Liu, Denys Makoviichuk, Karl Van Wyk, Alexander Zhurkevich, Balakumar Sundaralingam, and Yashraj Narang. [DeX-treme: Transfer of Agile In-hand Manipulation from Simulation to Reality](#). In *2023 IEEE International Conference on Robotics and Automation (ICRA)*, pages 5977–5984, 2023.
- [26] Nicklas Hansen, Hao Su, and Xiaolong Wang. [TD-MPC2: Scalable, Robust World Models for Continuous Control](#). In *The Twelfth International Conference on Learning Representations*, 2024.
- [27] Haoran He, Peilin Wu, Chenjia Bai, Hang Lai, Lingxiao Wang, Ling Pan, Xiaolin Hu, and Weinan Zhang. [Bridging the Sim-to-Real Gap from the Information](#)

- Bottleneck Perspective. In *8th Annual Conference on Robot Learning*, 2024.
- [28] Kaiming He, Xiangyu Zhang, Shaoqing Ren, and Jian Sun. [Deep Residual Learning for Image Recognition](#). In *2016 IEEE Conference on Computer Vision and Pattern Recognition (CVPR)*, pages 770–778, 2016.
- [29] Eric Heiden, Miles Macklin, Yashraj S Narang, Dieter Fox, Animesh Garg, and Fabio Ramos. [DiSECT: A Differentiable Simulation Engine for Autonomous Robotic Cutting](#). In *Proceedings of Robotics: Science and Systems*, Virtual, July 2021.
- [30] Eric Heiden, David Millard, Erwin Coumans, Yizhou Sheng, and Gaurav S. Sukhatme. [NeuralSim: Augmenting Differentiable Simulators with Neural Networks](#). In *2021 IEEE International Conference on Robotics and Automation (ICRA)*, pages 9474–9481, 2021.
- [31] Eric Heiden, Christopher E. Denniston, David Millard, Fabio Ramos, and Gaurav S. Sukhatme. [Probabilistic Inference of Simulation Parameters via Parallel Differentiable Simulation](#). In *2022 International Conference on Robotics and Automation (ICRA)*, pages 3638–3645, 2022.
- [32] Johannes Hertrich. [Fast Kernel Summation in High Dimensions via Slicing and Fourier Transforms](#). *SIAM Journal on Mathematics of Data Science*, 6(4):1109–1137, 2024.
- [33] Jonathan Ho, Ajay Jain, and Pieter Abbeel. [Denoising Diffusion Probabilistic Models](#). In H. Larochelle, M. Ranzato, R. Hadsell, M.F. Balcan, and H. Lin, editors, *Advances in Neural Information Processing Systems*, volume 33, pages 6840–6851. Curran Associates, Inc., 2020.
- [34] Victoria Hodge and Jim Austin. [A survey of outlier detection methodologies](#). *Artificial intelligence review*, 22:85–126, 2004.
- [35] David Hoeller, Nikita Rudin, Dhionis Sako, and Marco Hutter. [ANYmal parkour: Learning agile navigation for quadrupedal robots](#). *Science Robotics*, 9(88):eadi7566, 2024.
- [36] Geoffrey A Hollinger and Gaurav S Sukhatme. [Sampling-based Motion Planning for Robotic Information Gathering](#). In *Robotics: Science and Systems*, volume 3, pages 1–8, 2013.
- [37] Kai-Chieh Hsu, Vicenç Rubies-Royo, Claire Tomlin, and Jaime F Fisac. [Safety and Liveness Guarantees through Reach-Avoid Reinforcement Learning](#). In *Proceedings of Robotics: Science and Systems*, Virtual, July 2021.
- [38] Peide Huang, Xilun Zhang, Ziang Cao, Shiqi Liu, Mengdi Xu, Wenhao Ding, Jonathan Francis, Bingqing Chen, and Ding Zhao. [What went wrong? closing the sim-to-real gap via differentiable causal discovery](#). In *Conference on Robot Learning*, pages 734–760. PMLR, 2023.
- [39] Peide Huang, Xilun Zhang, Ziang Cao, Shiqi Liu, Mengdi Xu, Wenhao Ding, Jonathan Francis, Bingqing Chen, and Ding Zhao. [What Went Wrong? Closing the Sim-to-Real Gap via Differentiable Causal Discovery](#). In Jie Tan, Marc Toussaint, and Kourosh Darvish, editors, *Proceedings of The 7th Conference on Robot Learning*, volume 229 of *Proceedings of Machine Learning Research*, pages 734–760. PMLR, 06–09 Nov 2023.
- [40] Thomas Jaksch, Ronald Ortner, and Peter Auer. [Near-optimal Regret Bounds for Reinforcement Learning](#). *Journal of Machine Learning Research*, 11(51):1563–1600, 2010.
- [41] Fabian Jenelten, Junzhe He, Farbod Farshidian, and Marco Hutter. [DTC: Deep Tracking Control](#). *Science Robotics*, 9(86):eadh5401, 2024.
- [42] Yinsen Jia and Boyuan Chen. [ClutterGen: A Cluttered Scene Generator for Robot Learning](#). In *8th Annual Conference on Robot Learning*, 2024.
- [43] Josip Josifovski, Sayantan Auddy, Mohammadhossein Malmir, Justus Piater, Alois Knoll, and Nicolás Navarro-Guerrero. [Continual Domain Randomization](#). *arXiv preprint arXiv:2403.12193*, 2024.
- [44] Mihir Kulkarni, Theodor J. L. Forgaard, and Kostas Alexis. [Aerial Gym – Isaac Gym Simulator for Aerial Robots](#), 2023.
- [45] Joonho Lee, Marko Bjelonic, Alexander Reske, Lorenz Wellhausen, Takahiro Miki, and Marco Hutter. [Learning robust autonomous navigation and locomotion for wheeled-legged robots](#). *Science Robotics*, 9(89):eadi9641, 2024.
- [46] Yen-Chen Lin, Zhang-Wei Hong, Yuan-Hong Liao, Meng-Li Shih, Ming-Yu Liu, and Min Sun. [Tactics of adversarial attack on deep reinforcement learning agents](#). *arXiv preprint arXiv:1703.06748*, 2017.
- [47] Yuheng Liu, Xinke Li, Xueting Li, Lu Qi, Chongshou Li, and Ming-Hsuan Yang. [Pyramid diffusion for fine 3d large scene generation](#). In *European Conference on Computer Vision (ECCV)*, 2025.
- [48] Yecheng Jason Ma, William Liang, Hungju Wang, Sam Wang, Yuke Zhu, Linxi Fan, Osbert Bastani, and Dinesh Jayaraman. [DrEureka: Language Model Guided Sim-To-Real Transfer](#). In *Proceedings of Robotics: Science and Systems*, 2024.
- [49] Viktor Makoviychuk, Lukasz Wawrzyniak, Yunrong Guo, Michelle Lu, Kier Storey, Miles Macklin, David Hoeller, Nikita Rudin, Arthur Allshire, Ankur Handa, et al. [Isaac gym: High performance gpu-based physics simulation for robot learning](#). *arXiv preprint arXiv:2108.10470*, 2021.
- [50] Viraj Mehta, Ian Char, Joseph Abbate, Rory Conlin, Mark Boyer, Stefano Ermon, Jeff Schneider, and Willie Neiswanger. [Exploration via Planning for Information about the Optimal Trajectory](#). In S. Koyejo, S. Mohamed, A. Agarwal, D. Belgrave, K. Cho, and A. Oh, editors, *Advances in Neural Information Processing Systems*, volume 35, pages 28761–28775. Curran Associates, Inc., 2022.
- [51] Marius Memmel, Andrew Wagenmaker, Chuning Zhu, Dieter Fox, and Abhishek Gupta. [ASID: Active Explo-](#)

- ration for System Identification in Robotic Manipulation. In *The Twelfth International Conference on Learning Representations*, 2024.
- [52] Takahiro Miki, Joonho Lee, Jemin Hwangbo, Lorenz Wellhausen, Vladlen Koltun, and Marco Hutter. [Learning robust perceptive locomotion for quadrupedal robots in the wild](#). *Science Robotics*, 7(62):eabk2822, 2022.
- [53] Fabio Muratore, Theo Gruner, Florian Wiese, Boris Belousov, Michael Gienger, and Jan Peters. [Neural Posterior Domain Randomization](#). In Aleksandra Faust, David Hsu, and Gerhard Neumann, editors, *Proceedings of the 5th Conference on Robot Learning*, volume 164 of *Proceedings of Machine Learning Research*, pages 1532–1542. PMLR, 08–11 Nov 2022.
- [54] Duy P. Nguyen*, Kai-Chieh Hsu*, Wenhao Yu, Jie Tan, and Jaime Fernández Fisac. [Gameplay Filters: Robust Zero-Shot Safety through Adversarial Imagination](#). In *8th Annual Conference on Robot Learning*, 2024.
- [55] Tuomas Oikarinen, Wang Zhang, Alexandre Megretski, Luca Daniel, and Tsui-Wei Weng. [Robust Deep Reinforcement Learning through Adversarial Loss](#). In M. Ranzato, A. Beygelzimer, Y. Dauphin, P.S. Liang, and J. Wortman Vaughan, editors, *Advances in Neural Information Processing Systems*, volume 34, pages 26156–26167. Curran Associates, Inc., 2021.
- [56] Kei Ota, Devesh K. Jha, Diego Romeres, Jeroen van Baar, Kevin A. Smith, Takayuki Semitsu, Tomoaki Oiki, Alan Sullivan, Daniel Nikovski, and Joshua B. Tenenbaum. [Data-Efficient Learning for Complex and Real-Time Physical Problem Solving Using Augmented Simulation](#). *IEEE Robotics and Automation Letters*, 6(2): 4241–4248, 2021.
- [57] George Papamakarios and Iain Murray. [Fast \$\epsilon\$ -free inference of simulation models with Bayesian conditional density estimation](#). NIPS’16, page 1036–1044, Red Hook, NY, USA, 2016. Curran Associates Inc. ISBN 9781510838819.
- [58] Anay Pattanaik, Zhenyi Tang, Shuijing Liu, Gautham Bommannan, and Girish Chowdhary. [Robust Deep Reinforcement Learning with Adversarial Attacks](#). Richland, SC, 2018. International Foundation for Autonomous Agents and Multiagent Systems.
- [59] Lerrel Pinto, James Davidson, Rahul Sukthankar, and Abhinav Gupta. [Robust Adversarial Reinforcement Learning](#). In Doina Precup and Yee Whye Teh, editors, *Proceedings of the 34th International Conference on Machine Learning*, volume 70 of *Proceedings of Machine Learning Research*, pages 2817–2826. PMLR, 06–11 Aug 2017.
- [60] Fabio Ramos, Rafael Possas, and Dieter Fox. [BayesSim: Adaptive Domain Randomization Via Probabilistic Inference for Robotics Simulators](#). In *Proceedings of Robotics: Science and Systems*, Freiburg/Breisgau, Germany, June 2019.
- [61] Allen Z. Ren, Hongkai Dai, Benjamin Burchfiel, and Anirudha Majumdar. [AdaptSim: Task-Driven Simulation Adaptation for Sim-to-Real Transfer](#). In Jie Tan, Marc Toussaint, and Kourosh Darvish, editors, *Proceedings of The 7th Conference on Robot Learning*, volume 229 of *Proceedings of Machine Learning Research*, pages 3434–3452. PMLR, 06–09 Nov 2023.
- [62] John Schulman, Filip Wolski, Prafulla Dhariwal, Alec Radford, and Oleg Klimov. [Proximal Policy Optimization Algorithms](#), 2017.
- [63] John Schulman, Filip Wolski, Prafulla Dhariwal, Alec Radford, and Oleg Klimov. [Proximal policy optimization algorithms](#). *arXiv preprint arXiv:1707.06347*, 2017.
- [64] Pier Giuseppe Sessa, Maryam Kamgarpour, and Andreas Krause. [Efficient model-based multi-agent reinforcement learning via optimistic equilibrium computation](#). In *International Conference on Machine Learning*, pages 19580–19597. PMLR, 2022.
- [65] Louis Sharrock, Jack Simons, Song Liu, and Mark Beaumont. [Sequential Neural Score Estimation: Likelihood-Free Inference with Conditional Score Based Diffusion Models](#). In *Forty-first International Conference on Machine Learning*, 2024.
- [66] Fan Shi, Chong Zhang, Takahiro Miki, Joonho Lee, Marco Hutter, and Stelian Coros. [Rethinking Robustness Assessment: Adversarial Attacks on Learning-based Quadrupedal Locomotion Controllers](#). In *Proceedings of Robotics: Science and Systems*, Delft, Netherlands, July 2024.
- [67] S. A. Sisson, Y. Fan, and Mark M. Tanaka. [Sequential Monte Carlo without likelihoods](#). *Proceedings of the National Academy of Sciences*, 104(6):1760–1765, 2007.
- [68] Sriram Siva, Maggie Wigness, John Rogers, and Hao Zhang. [Enhancing Consistent Ground Maneuverability by Robot Adaptation to Complex Off-Road Terrains](#). In *5th Annual Conference on Robot Learning*, 2021.
- [69] Yang Song, Jascha Sohl-Dickstein, Diederik P Kingma, Abhishek Kumar, Stefano Ermon, and Ben Poole. [Score-Based Generative Modeling through Stochastic Differential Equations](#). In *International Conference on Learning Representations*, 2021.
- [70] Sarath Sreedharan and Michael Katz. [Optimistic exploration in reinforcement learning using symbolic model estimates](#). *Advances in Neural Information Processing Systems*, 36:34519–34535, 2023.
- [71] Kyle Stachowicz and Sergey Levine. [RACER: Epistemic Risk-Sensitive RL Enables Fast Driving with Fewer Crashes](#). In *Proceedings of Robotics: Science and Systems*, Delft, Netherlands, July 2024.
- [72] Kyle Stachowicz, Lydia Ignatova, and Sergey Levine. [Lifelong Autonomous Improvement of Navigation Foundation Models in the Wild](#). In *8th Annual Conference on Robot Learning*, 2024.
- [73] Bhavya Sukhija, Lenart Treven, Cansu Sancaktar, Sebastian Blaes, Stelian Coros, and Andreas Krause. [Optimistic Active Exploration of Dynamical Systems](#). In A. Oh, T. Naumann, A. Globerson, K. Saenko, M. Hardt, and S. Levine, editors, *Advances in Neural Information*

- Processing Systems*, volume 36, pages 38122–38153. Curran Associates, Inc., 2023.
- [74] Gabriele Tiboni, Andrea Protopapa, Tatiana Tommasi, and Giuseppe Averta. [Domain Randomization for Robust, Affordable and Effective Closed-Loop Control of Soft Robots](#). In *2023 IEEE/RSJ International Conference on Intelligent Robots and Systems (IROS)*, pages 612–619, 2023.
- [75] Josh Tobin, Rachel Fong, Alex Ray, Jonas Schneider, Wojciech Zaremba, and Pieter Abbeel. [Domain randomization for transferring deep neural networks from simulation to the real world](#). In *2017 IEEE/RSJ international conference on intelligent robots and systems (IROS)*, pages 23–30. IEEE, 2017.
- [76] Emanuel Todorov, Tom Erez, and Yuval Tassa. [MuJoCo: A physics engine for model-based control](#). In *2012 IEEE/RSJ International Conference on Intelligent Robots and Systems*, pages 5026–5033. IEEE, 2012.
- [77] Lenart Treven, Cansu Sancaktar, Sebastian Blaes, Stelian Coros, and Andreas Krause. [Optimistic active exploration of dynamical systems](#). *Advances in Neural Information Processing Systems*, 36:38122–38153, 2023.
- [78] Ya-Yen Tsai, Hui Xu, Zihan Ding, Chong Zhang, Edward Johns, and Bidan Huang. [DROID: Minimizing the Reality Gap Using Single-Shot Human Demonstration](#). *IEEE Robotics and Automation Letters*, 6(2):3168–3175, 2021.
- [79] A Vaswani. [Attention is all you need](#). *Advances in Neural Information Processing Systems*, 2017.
- [80] Marcel Torne Villasevil, Anthony Simeonov, Zechu Li, April Chan, Tao Chen, Abhishek Gupta, and Pulkit Agrawal. [Reconciling Reality through Simulation: A Real-To-Sim-to-Real Approach for Robust Manipulation](#). In *Proceedings of Robotics: Science and Systems*, Delft, Netherlands, July 2024.
- [81] Jane X Wang, Zeb Kurth-Nelson, Dhruva Tirumala, Hubert Soyer, Joel Z Leibo, Remi Munos, Charles Blundell, Dhharshan Kumaran, and Matt Botvinick. [Learning to reinforcement learn](#). *arXiv preprint arXiv:1611.05763*, 2016.
- [82] Fan Yang, Chen Wang, Cesar Cadena, and Marco Hutter. [iPlanner: Imperative Path Planning](#). In *Proceedings of Robotics: Science and Systems*, Daegu, Republic of Korea, July 2023.
- [83] Youwei Yu, Junhong Xu, and Lantao Liu. [Adaptive Diffusion Terrain Generator for Autonomous Uneven Terrain Navigation](#). In *8th Annual Conference on Robot Learning*, 2024.
- [84] Zongsheng Yue, Jianyi Wang, and Chen Change Loy. [Efficient Diffusion Model for Image Restoration by Residual Shifting](#). *IEEE Transactions on Pattern Analysis and Machine Intelligence*, 47(1):116–130, 2025.
- [85] Ji Zhang, Chen Hu, Rushat Gupta Chadha, and Sanjiv Singh. [Falco: Fast likelihood-based collision avoidance with extension to human-guided navigation](#). *Journal of Field Robotics*, 37:1300 – 1313, 2020.
- [86] Ziwen Zhuang, Zipeng Fu, Jianren Wang, Christopher G Atkeson, Sören Schwertfeger, Chelsea Finn, and Hang Zhao. [Robot Parkour Learning](#). In *Conference on Robot Learning*, 2023.
- [87] Ziwen Zhuang, Shenzhe Yao, and Hang Zhao. [Humanoid Parkour Learning](#). In *8th Annual Conference on Robot Learning*, 2024.

APPENDIX

A. Radial Kernel

We introduce the basic ideas of using radial kernels for feature representation.

1) *Radial Basis Function*: For inputs $x \in \mathbb{R}^d$ and $y \in \mathbb{R}^d$, the radial basis function (RBF) takes the radial kernels $K(x, y) = F(\|x - y\|)$ with the symmetric basis function $F(\cdot) : \mathbb{R}_{\geq 0} \rightarrow \mathbb{R}$. We list some well-known kernels:

- Gaussian: $F(x) = \exp\left(-\frac{x^2}{2\sigma^2}\right)$.
- Laplacian: $F(x) = \exp(-\alpha x)$.
- Matérn: $F(x) = \frac{2^{1-\nu}}{\Gamma(\nu)} \left(\sqrt{\frac{2\nu}{\beta}} x\right)^\nu K_\nu\left(\sqrt{\frac{2\nu}{\beta}} x\right)$.

For scaling to large numbers of training samples or high-dimensional states, Random Fourier Feature (RFF) and Fast Kernel Summation (FKS) can approximate RBF.

2) *Random Fourier Feature*: Let $K : \mathbb{R}^d \times \mathbb{R}^d \rightarrow \mathbb{R}$ be given by $K(x, y) = \Psi(x - y)$, a bounded shift-invariant positive definite kernel with $K(x, x) = \Psi(0) = 1$. Then it holds by Bochner’s theorem that there exists a probability measure μ on \mathbb{R}^d such that

$$\begin{aligned} \Psi(x - y) &= \hat{\mu}(x - y) = \mathbb{E}_{v \sim \mu} [\exp(2\pi i \langle x - y, v \rangle)] \\ &= \mathbb{E}_{v \sim \mu} [\exp(2\pi i \langle x, v \rangle) \exp(-2\pi i \langle y, v \rangle)]. \end{aligned} \quad (15)$$

Random Fourier Feature (RFF) simply puts $y = 0$,

$$\Psi(x) = \mathbb{E}_{v \sim \mu} [\exp(2\pi i \langle x, v \rangle)]. \quad (16)$$

Taking Euler’s formula and the real parts, we have

$$\Psi(x) = \mathbb{E}_{b \sim U[0, 2\pi]} [\cos(\langle x, v \rangle) + \sin(\langle x, v \rangle)]. \quad (17)$$

3) *Fast Kernel Slicing*: We briefly delineate fast kernel slicing (FKS) methods [32] that reduce high-dimensional problems to the one-dimensional case by projecting the points of interest onto lines in directions ξ which are uniformly distributed on the unit sphere $\mathbb{S}^{P-1} \subset \mathbb{R}^P$. In this paper, we assume the kernel $K : \mathbb{R}^d \times \mathbb{R}^d \rightarrow \mathbb{R}$ has the form:

$$K(x, y) = \mathbb{E}_{\xi \sim \mathcal{U}_{\mathbb{S}^{P-1}}} [k(\langle \xi, x \rangle, \langle \xi, y \rangle)] \quad (19)$$

with the one-dimensional kernel $k : \mathbb{R} \times \mathbb{R} \rightarrow \mathbb{R}$ and uniform distribution \mathcal{U} . For radial kernels $K(x, y) = F(\|x - y\|)$ with some basis function $F : \mathbb{R}_{\geq 0} \rightarrow \mathbb{R}$, with the notation $L_{\text{loc}}^\infty := \{f : \mathbb{R}_{\geq 0} : f|_{[0, s]} \in L^\infty([0, s]), \forall s > 0\}$. Then the basis function of K can be expressed by the *generalized Riemann-Liouville fractional integral* transform defined by

$$\begin{aligned} \mathcal{S}_d : L_{\text{loc}}^\infty &\rightarrow L_{\text{loc}}^\infty, \quad \mathcal{S}_d(f) = F \\ F(s) &= \frac{2\Gamma(\frac{d}{2})}{\sqrt{\pi}\Gamma(\frac{d-1}{2})} \int_0^1 f(ts)(1-t^2)^{\frac{d-3}{2}} dt \end{aligned} \quad (20)$$

This can be done explicitly if

- 1) F is an analytic function with globally convergent Taylor series in 0 given by $F(x) = \sum_{n=0}^\infty a_n x^n$.

To subsample the expectations, let $\{v_1, \dots, v_D\}$ be i.i.d. samples from μ and $\{b_1, \dots, b_D\}$ be i.i.d. samples from $U[0, 2\pi]$, we have

$$\text{RFF}(x) = \{\cos(\langle x, v_p \rangle + b_p), \sin(\langle x, v_p \rangle + b_p)\}_{p=1}^D \quad (18)$$

- 2) F is continuous, bounded, and positive definite, i.e., for all $i \in \{1, \dots, n\}$ with $n \in \mathbb{N}$, it holds that $\sum_{i,j=1}^n a_i a_j F(\cdot) \geq 0$.

Thus we can get the P features via projections and the one-dimensional basis function with weights w

$$\text{FKS}(x) = \{w_p f(\langle \xi_p, x \rangle)\}_{p=1}^D \quad (21)$$

whose computation complexity is $\mathcal{O}(D \times \dim(\tau^{\text{latent}}))$. The expected error of slicing can be bounded by $\mathcal{O}(1/\sqrt{D})$. For a fair comparison to RFF, we assign 1024 features with Quasi-Monte Carlo simulation to both methods and uniform weights to the robot trajectory.

B. System Implementations

1) *Network Architecture*: ResNet-18 [28] extracts 1024 features from the elevation map $e \in \mathbb{R}^{128 \times 128}$, while Causal TCN is structured with channel sizes [256, 128, 64, 16]. The resulting feature representations are concatenated and passed through a linear layer, mapping them to 1024 features. These features are then fed into an SDE-based Diffusion model [65] to infer simulator calibration parameters, residual dynamics, and residual environment parameters. For action generation, we use an MLP with layer sizes [1024, 512, 2] for the wheeled robot, where the 2 output dimension can be adjusted for other robots as needed.

2) *Sim-to-Sim Experiment Domains*: We detail the simulator physical domains for Ant, Quadruped, Humanoid, Quadcopter, and Jackal.

<hr/>		
Ant		
mass	8	4 legs, 4 feet
stiffness	13	5 torsos, 4 ankles, 4 hips
<hr/>		
Quadruped		
mass	9	1 base, 4 thighs, 4 shanks
stiffness	4	4 hips
<hr/>		
Humanoid		
mass	20	
stiffness	17	
<hr/>		
Quadcopter		
mass	5	1 chassis, 4 arms
stiffness	4	4 rotors
<hr/>		
Jackal		
mass	5	1 base, 4 wheels
damping	4	4 wheels
friction	4	4 wheels
restitution	4	4 wheels
<hr/>		

Refer to IsaacGym [49] for the detailed description of Humanoid and other robots.